The concentration-dependent effect of hydrocortisone on the structure of model lung surfactant monolayer by using an in-silico approach

Mohammad Zohurul Islam[1], Sheikh I. Hossain[2], E. Deplazes[2,a], Zhen Luo[1] and Suvash C. Saha[1, a]

[1]*School of Mechanical and Mechatronic Engineering, University of Technology Sydney, 15 Broadway, Ultimo, NSW 2007, Australia*
[2]*School of Life Sciences, University of Technology Sydney, 15 Broadway, Ultimo, NSW 2007, Australia*

[a] co-corresponding authors: Suvash.Saha@uts.edu.au and Evelyne.Deplazes@uts.edu.au

Abstract

Understanding the adsorption mechanism of corticosteroid in the lung surfactant requires the knowledge of corticosteroid molecular interactions with lung surfactant monolayer (LSM). We employed coarse-grained molecular dynamics simulation to explore the action of hydrocortisone on a LSM comprised of phospholipid, cholesterol and surfactant protein. The structural and dynamical morphology of the lung surfactant monolayer at different surface tensions were investigated to assess the monolayer compressibility. The simulations were also conducted at the two extreme ends of breathing cycles, such as exhalation (0 mNm^{-1} surface tension) and inhalation (20 mNm^{-1} surface tension). The impact of surface tension and hydrocortisone concentration on the monolayer compressibility as well as stability are significant, resulting in the monolayer expansion at higher surface tension. However, at low surface tension producing the highly compressed monolayer induces monolayer instability in the presence of drug due to the accumulation of surfactant protein and drug. The constant area per lipid simulation results demonstrate that the surface pressure-area isotherms show a decrease in area-per-lipid with the increase of drug concentration. The drug-induced expansion causes considerable instability in the monolayer after a specific drug concentration is attained at inhalation breathing condition, whereas, for exhalation breathing, the monolayer gets more compressed, causing the LSM to collapse. The monolayer collapse occurs for inhalation due to the higher drug concentration, whereas for exhalation due to the accumulation of surfactant proteins and drugs. The findings from this study will aid to enhance the knowledge of molecular interactions of corticosteroid drug with lung surfactant to treat respiratory diseases.

Keywords: Corticosteroids; Hydrocortisone; Lung surfactant monolayer; Molecular dynamics simulation; Surface tension

1 Introduction

Hydrocortisone is a glucocorticoid that is used as an anti-inflammatory and immunosuppressive drug to treat a range of inflammatory and allergy conditions [1, 2], including many pulmonary illnesses such as asthma, chronic obstructive pulmonary disease, influenza and bronchitis [3], and bronchopulmonary dysplasia in infants [4-6]. A recent study conducted by Petersen *et al*., [7] also showed that corticosteroids, including hydrocortisone, reduce the amount of mechanical ventilation required by patients with severe acute respiratory syndrome caused by SARS-COV-2. Hydrocortisone might be as useful as dexamethasone to treat covid-19 [8].

Normal breathing and lung function rely on the activity of lung surfactant, which are secreted and synthesised from alveolar type II cell, and create a bilayer-associated monolayer at the alveolar air-water interface [9-11] known as the lung surfactant monolayer (LSM). The functions of LSM include supporting the mechanical work of breathing by dropping the surface tension and preventing alveolar collapse at exhalation when surface tension reaches values close to zero [12-14]. The LSM serves as the first line of defense against potential inhaled pathogens/particles entering the lung, and of course the same barrier also protects again many inhaled entities.

All of these functions, interfacial surface area regulation and compressibility of the lung surfactant are highly dependent on the lung surfactant composition, surfactant molecules organisation at air-liquid interface in the alveoli [15]. Lack of surfactant or any imbalance of surfactant can cause reduced lung surfactant activity. In mammalian lung surfactants, phospholipids are the most abundant component comprising approximately 85% by weight [16]. Of the phospholipids, the zwitterionic phosphatidylcholine (PC) lipids are the most abundant species amounting to ~70% w/w. More than 50% of total PC lipids is di-saturated 1, 2-dipalmitoyl-sn-glycero-3-phosphatidylcholine (DPPC), and the remaining species are either mono or di-unsaturated phospholipids such as 1-palmitoyl-2-oleoyl-sn-glycero-3-phosphocholine (POPC) [17, 18]. The next common phospholipids, account for ~10% w/w, are negatively charged phosphatidylglycerol (PG) lipids such as 1-palmitoyl-2-oleoyl-sn-glycero-3-phosphoglycerol (POPG) or 1,2-dipalmitoyl-sn-glycero-3-phosphoglycerol (DPPG) [10, 15, 19]. In addition to phospholipids, the LSM also contains nearly ~8% cholesterol (CHOL) [15]. Besides lipids, the LSM contains ~8% surfactant protein [20, 21]. They are divided into two categories: hydrophilic proteins (SP-A and SP-D) that are found in the aqueous subphase of the lipid bilayer, and hydrophobic proteins (SP-B and SP-C) that are anchored in the membrane involving the surface-tension regulating activity of the LSM [22, 23].

During regular breathing, the LSM is continuously compressed and expanded. The surface tension lies between ≈ 0 mNm^{-1} near the end of exhalation, at maximal compression, and between 20-25 mNm^{-1} during inhalation, at maximal expansion [12, 24] of the monolayer. As a result of this compression and expansion properties, the LSM passes through different phases; liquid-condensed (LC) phase, a transitional phase (LC + LE), in which the LC and liquid-expanded phase (LE) coexist and liquid-expanded phase (LE) [25, 26] of the monolayer. The structure and thus phase behaviour of the LSM is strongly related to the packing and movement of lipids in the monolayer. The phase behaviour of the monolayer can be expressed in a function of the surface pressure and surface tension according to the equation $\pi = \gamma_{a\text{-}w} - \gamma_{eq}$, where, π is the pressure, $\gamma_{a\text{-}w}$ (~72 mNm^{-1} at 310 K) is the surface tension of the pure water at the air-water interface, and γ_{eq} is the surface tension of the monolayer. Monolayer phase transition from LC phase to LE phase induced from the high surface pressure to low surface pressure, respectively. Due to the complexity of the LSM and changing the structure of LSM during breathing cycles, understanding the interaction of inhaled drug such as corticosteroid drugs is not trivial. As each phase shows different lipid packing, compressibility and surface tension, the interaction of drug with LSM is not only dependent on the drug concentration but also on the LSM phase. Nevertheless, elucidating these interactions is important to understand how corticosteroid drugs are adsorbed into the LSM.

Understanding the interactions of lung surfactants with corticosteroids is also important for improving drug delivery to treat pulmonary illnesses. The lack and dysfunction of lung surfactants is linked to severe respiratory diseases [27]. In some cases, treatment includes exogenous surfactants, which also might include the addition of corticosteroids [28]. Furthermore, delivery of corticosteroid to the alveoli and their incorporation into endogenous lung surfactants might be improved by incorporating the drug into exogenous surfactants [29]. While the main therapeutic target of corticosteroids are receptors, inhaled drugs can reach the LSM where they alter the structure and dynamics of the monolayer with detrimental effects on normal lung function. Thus, exogenous lung surfactants might not only improve corticosteroid delivery but also reduce side effects of inhaled glucocorticoids. To understand how corticosteroid drugs can be incorporated into exogenous surfactants, the molecular interactions between the drug and surfactants is critical.

The interaction of the corticosteroids such as beclomethasone, budesonide and fluticasone with exogenous lung surfactant was investigated by Cimato *et al*., [30]. They explored the concentration-dependent effect of these three corticosteroids as well as cholesterol on

surfactant fluidity and compressibility using pulsating bubble surfactometer and polarised microscopy experiment. In the absence of corticosteroids or cholesterol, the monolayer formed by exogenous lung surfactants showed a film compressibility of 60%. This was reduced to less than 40% in the presence of the drugs or cholesterol. These results also show that at low compressibility, the LSM can decrease surface tension to less than 2 mNm^{-1}, which is close to the 0 mNm^{-1} required for normal breathing. A similar surface tension lowering capabilities were also reported by other biophysical studies for corticosteroid containing natural and exogenous surfactant [31, 32]. This experimental study also demonstrates that at lower drug concentration the drug does not destabilise the surfactant monolayer. Cimato *et al*., [33] conducted an experimental study to investigate the corticosteroid-associated lung surfactant formulation to advance the spreading mechanism of corticosteroid. In their study, the authors explored corticosteroid budesonide interaction with exogenous pulmonary surfactant to advance the drug delivery to the alveoli. In an study conducted by Wang *et al*., [32] combined the Langmuir balance and AFM experiments to investigate the corticosteroid interaction with commercially available natural surfactant (Infasurf) and two corticosteroid (budesonide and beclomethasone propionate) drugs. The characteristic isotherms of Infasurf at 0.1, 1, and 10% budesonide and beclomethasone propionate were compared to investigate the corticosteroid effects on the activity of the monolayer. Budesonide and beclomethasone propionate do not significantly interfere with the Infasurf monolayer stability up to corticosteroid concentrations of $\leq$ 1% w/w for budesonide and $\leq$ 10% w/w for beclomethasone propionate. Once these concentrations were exceeded, the corticosteroids induce instability of the monolayer due to monolayer fluidisation. Thus, Infasurf loaded with drug below the above-mentioned critical concentration of drug could be useful to measure the spreading of corticosteroids to the lung surfactant correctly at the alveolar air-water surface.

To investigate how corticosteroid drug budesonide affects monolayer biophysics including monolayer fluidity and surface pressure, Dos Santos *et al*., [34] performed an *in vitro* experimental study using the monolayer composition POPC-DOPC-CHOL in the presence of budesonide and budesonide mixed Cyclodextrin oligosaccharides complex. The study demonstrated that cholesterol changes the lipid packing and lipid desorption with the help of corticosteroid drug budesonide. Budesonide increased membrane fluidity and permeability according to their findings. It is also found that budesonide induced the disruption of lipid monolayer in cholesterol-enriched raft-like domains that change the lipid packing in monolayer. In addition to the above-mentioned studies, a wide range of wet-lab methods has

also been investigated to study the structure and physicochemical characteristics of the LSM, including Langmuir trough [35-40], atomic force microscopic (AFM) [32], electron resonance spectroscopy [30] and captive bubble surfactometer experiments [41]. These techniques can also be used to study the interaction of the LSM with steroids [42-44] and non-steroid drugs [45-47], but they do not provide proper molecular-level mechanistic interaction between drugs and LSM. To precisely understand the molecular level mechanistic interaction of corticosteroid drugs and surfactant monolayer, it is preferable to use coarse-grained lung surfactant models.

Computer simulation is one of the techniques to study the structural and dynamical properties of LSM. This method has been used to investigate the stability and biophysical characteristics of lung surfactant monolayers and bilayers. The interaction of the corticosteroid drug prednisolone with a simple model LSM was investigated by Estrada-López *et al.*, [48] using a coarse-grained (CG) MD simulations at surface tension 0, 10 and 20 mNm^{-1}. Results revealed that the film collapses at low surface tensions (0 mNm^{-1}). In a recent study, the CG MD simulation was used to investigate the effect of mometasone on a LSM model comprised of DPPC-POPC-POPG-CHOL and surfactant protein (SP-B and SP-C) containing monolayer [42]. The results revealed that mometasone alters the structure of the LSM as a function of drug concentration, and causes monolayer to collapse, which is influenced by surface tension and surfactant protein. The accumulation of drug molecules limits the drug capacity to spread into the surfactant monolayer at high drug concentration, resulting monolayer collapse. The findings from these studies highlight the complexity of these systems and specify the impact of corticosteroid is facilitated by specific interactions between the drug and surfactants. The drug-induced changes in surfactant properties are concentration-dependent and rely on lipid composition, surface tension or alternatively surface pressure.

However, molecular interactions with corticosteroids from such experiments are little known, and more research into lung surfactant stability and mechanical properties is needed to figure out how to distribute corticosteroid drugs into the targeted region of the alveoli by avoiding lung surfactant damage. Drug interaction with lung surfactants has contributed to the development of more efficient and less intrusive ways for a therapeutic dose, controllable corticosteroid release, and off-targeting drug deposition on LSM [49].

In this study, the CG MD simulations is used to investigate the minimum and maximum compressibility of the LSM for the drug-free and drug-containing monolayer by constant surface tension simulation ranging from 0 to 50 mNm^{-1}. The mechanistic changes of the LSM at inhalation (20 mNm^{-1}) and exhalation (0 mNm^{-1}) breathing

conditions for different drug concentration is also investigated. The broader ranges of surface tensions beyond the exhalation and inhalation surface tension are used to investigate the extremum APL values (lowest and highest APL) of the LSM and their phase analysis. To analyse phase behaviour of the LSM and monolayer-to-multilayer transformation of the LSM at LC and LE phases, the fixed APL simulation were carried out at APL values ranging from 0.47 to 0.61 nm^2. Finally, to isolate the effect of hydrocortisone concentration on breathing dynamics, the drug containing systems were simulated at exhalation breathing (0 mNm^{-1}) and inhalation breathing (20 mNm^{-1}). For all the underlying LSM model used in this study is composed of DPPC-POPC-POG-CHOL (60:20:10:10) and surfactant protein (SP-B-SP-C, 1:1) to mimic the fraction of surfactant components observed in human lung surfactants [19]. This amount of surfactant molecules ensures the trustworthy composition of LSM in mol% [15-21] that equivalent to the number of surfactant molecules, 65% DPPC, 21% POPC, 5% POPG, 5% CHOL and 4% surfactant proteins (SP-B and SP-C) by mass.

2 Methodology

2.1 Simulation parameter and simulation model setup

The monolayer was built by using two symmetric lipid-protein monolayers of dimensions 25.0 × 25.0 × 60.0 nm^3 that were put into a water box of dimensions 25.0 × 25.0 × 12.0 nm^3. Monolayers were spaced sufficiently far apart to avoid the interaction between them (Fig. 1a). Each monolayer is comprised of 2032 phospholipids and cholesterol molecules at a molar ratio DPPC-POPC-POPG-CHOL (60:20:10:10) with surfactant protein B and C (SP-B and SP-C, 1:1). Sixteen (16) monolayer-associated surfactant proteins (8 SP-B and 8 SP-C) were incorporated into the monolayer. The number of water beads was ~50,000. The monolayers were built by using the python script *insane.py* [50] according to the protocol stated by Hossain *et al*., [51]. The CG parameters for DPPC, POPC, POPG, CHOL and water were obtained standard MARTINI force field [52-56]. The CG structure of DPPC, POPC, POPG, CHOL, SP-B, SP-C and hydrocortisone are represented in Fig. S1 and Fig. 1b, c. The structure of the surfactant proteins (SP-B and SP-C) were based on the all-atom structure of SP-B from protein data bank (PDB ID:1DFW [57]) and SP-C (PDB ID: 1SPF [58]). For $SP\text{-}B_{1\text{-}25}$ sequence,

FPIPLPYCWLCRALIKRIQAMIPKG was chosen [59-62]. For SP-C, the sequence LRIPCCPVNLKRLLVVVVVVVLVVVVIVGALLMGL was used that contains 35-residues containing the 23 hydrophobic residues showing activities in LSM surface [63, 64]. The net charge of SP-B_{1-25} and SP-C model are +4 and +3 [64]. The python script *matinize.py* was used to convert the protein structures from all-atoms to CG. The CG topology of hydrocortisone was described based on other sterols/steroids previously reported [48, 65] and using standard MARTINI beads [56]. The detailed description of the topology and bead types of hydrocortisone are found in the supplementary section (S1.1, Table S1 and Fig. 1b, c). The hydrocortisone parameter was validated by calculating the ocatnol-water partition coefficient from free energy required to move the drug molecule from an octanol phase into the water phase. The free energy was achieved from a potential mean force (PMF) calculation using standard umbrella sampling simulations. The detailed procedure of these measurement is described in the supplementary material (S1.2).

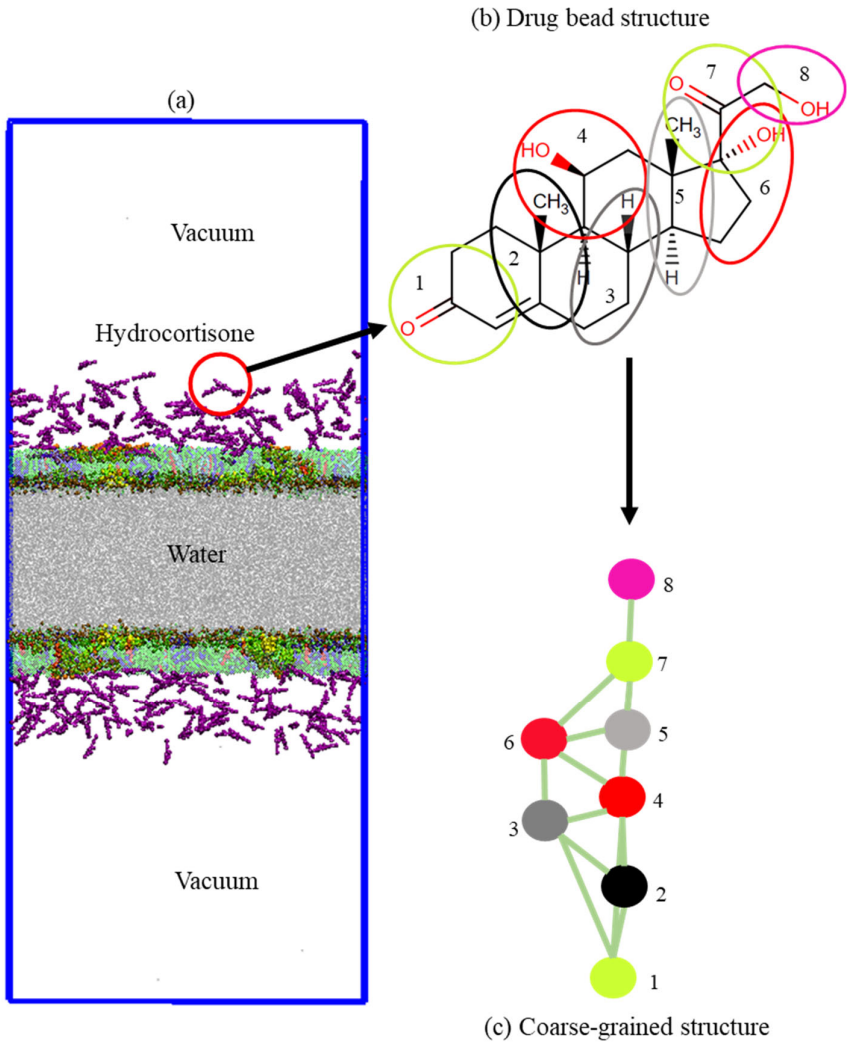

Figure 1. (a) Representation of the system composed surfactant components in the presence of hydrocortisone molecules. The system consists of two surfactant monolayers detached by a 12 nm water box, and 21 nm vacuum on each side of the layer. The monolayer is comprised of DPPC, POPC, POPG and cholesterol with surfactant proteins B and C (SP-B and SP-C). The system components are indicated by DPPC (green), POPC (blue), POPG (cyan), cholesterol (red) and hydrocortisone (purple), SP-$B_{1\text{-}25}$ (yellow), SP-C (orange) and water (silver). (b) Chemical structure of hydrocortisone and (c) Coarse grained bead representation of hydrocortisone.

2.2 Molecular dynamics simulation

2.2.1 Simulation systems for fixed surface tension and fixed APL

A reference system (Table 1) of drug-free monolayer comprised of DPPC:POPC:POPG:CHOL:SP-$B_{1\text{-}25}$:SP-C (60:20:10:10:1:1) was simulated at NPγT ensemble using surface tensions ranging from 0 to 50 mNm^{-1} with an interval of 10 mNm^{-1} to reproduce highly compressed (0 mNm^{-1}) to highly expanded (50 mNm^{-1}) monolayers (system I). Monolayers with eight different APL values of 0.47, 0.49 0.51, 0.53, 0.55, 0.57, 0.59 and 0.61 nm^2 were extracted from previously built reference systems. These monolayers were inserted into a simulation box with dimensions 24.90×24.90 nm^2, 24.49×24.49 nm^2, 24.10×24.10 nm^2, 23.64×23.64 nm^2, 23.21×23.21 nm^2, 22.77×22.77 nm^2 and 22.32×22.32 nm^2, respectively to ensure APL values remain at the target APL values during NVT simulations. Each of these eight systems (system II) was equilibrated first 500 ns and then 2 μs final simulation in the NVT ensemble.

For simulation of the hydrocortisone containing LSM, five different models were setup. The original configurations of the drug-containing system were collected from the final trajectories of the corresponding reference conformation from the fixed surface tension simulation (system I) and fixed APL simulation (system II). The hydrocortisone molecules were arbitrarily inserted in air phase of the system as shown in Fig. 1a. These five drugs containing systems were equilibrated 500 ns followed by a 2 μs production run in the NVT ensemble for fixed APL (system II) simulation. For fixed surface tension simulation, each of the five drug-LSM systems was equilibrated for 500 ns in an NVT ensemble, followed by further equilibration in an NPγT ensemble, and final 2 μs production run simulation for data analysis. The NPγT were carried out at 0 mNm^{-1} and 20 mNm^{-1} surface tension.

Table 1. List of 136 simulation systems composed of DPPC:POPC:POPG:CHOL (60:20:10:10) and surfactant proteins (SP-B_{1-25} and SP-C, 1:1) in the presence of hydrocortisone (0 to ~10.5% w/w). The systems are simulated at NPγT and NVT ensemble. $N_{hydrocortisone}$ refers the number of hydrocortisone molecule per leaflet of the monolayer. Each of all systems were simulated at least two repeated runs.

System	$N_{hydrocortisone/monolayer}$	Concentration (% w/w)
NPγT simulation at surface tension: γ=0, 10, 20, 30, 40 and 50 mNm^{-1} (system I)		
I	0	0%
	120	5.52%
NVT simulation at fixed APL: 0.47, 0.49, 0.51, 0.53, 0.55, 0.57, 0.59 and 0.61 nm^2 (system II)		
II	0	0%
	10	0.49%
	30	1.44%
	60	2.84%
	120	5.52%
	240	10.46%
NPγT simulation at surface tension: γ=0 and 20 mNm^{-1} (system III)		
III	0	0%
	10	0.49%
	30	1.44%
	60	2.84%
	120	5.52%
	240	10.46%

GROMACS version 5.1.4 [66] was used to simulate all the systems. Each system was energy minimised using the steep descent algorithm. The leapfrog algorithm [67] with a 20 fs time step was used. The Martini standard cut-off for coulomb interaction potential and Lennard-Jones interaction were taken. Monolayer components (proteins, lipids and cholesterol), water and ions, and hydrocortisone were coupled independently at a temperature of 310 K with a V-rescale thermostat [68] and a time constant of τ=1.0 ps. The Berendsen barostat [69] at temperature 310 K was used with τ = 4.0 ps. The compressibility along the *xy*-plane and z-axis were fixed 4.5 $\times 10^{-5}$ bar^{-1} and zero, respectively. The neighbour lists were updated for each 20 steps.

2.2.2. Data Analysis and visualisation

All trajectories from the last 1 μs of the 2 μs simulation were extracted for analysis, and properties were averaged over the repeated runs of the simulations, unless otherwise stated. All

analyses were accomplished using GROMACS tools and customised python scripts. The visual molecular dynamics (VMD [70]) and the tcl script *cg_bonds-v5.tcl* [71] was used to render the CG MARTINI bonds and visualise the simulations. The python script: *do-ordergmx5.py* [71] was used to calculate lipid order parameters. The analysis was done by calculating APL, surface tension, lipid order parameters, clustering, and diffusion analyses of the dug and surfactant molecules, which are outlined in this study.

3 Results and discussion

The aims of this study were to examine the minimum and maximum compressibility for monolayer phase analysis and the concentration-dependent effect of hydrocortisone on the structural properties of the LSM. For this, the simulations were run in absence and presence of five different hydrocortisone concentrations from 0% to 10.50% w/w (Table 1). For drug-free case, the LSM was simulated at a range of fixed surface tension simulation (0 to 50 mNm^{-1}) to get the initial trajectories from fixed APL simulation. Each drug containing system was simulated in two different conditions inhalation (20 mNm^{-1}) and exhalation (0 mNm^{-1}) breathing. For fixed APL simulation, there are eight different APL values representing the range of compressibility of the LSM during the breathing cycle. The fixed surface tension simulations representing the expanded and compressed LSM were conducted at the extreme ends of breathing cycles; 20 mNm^{-1} for the end state of inhalation and 0 mNm^{-1} for the end state of exhalation. Hydrocortisone concentrations are chosen to the ones that used in existing biophysical studies of corticosteroids [42, 48, 72].

3.1 Monolayer compressibility and stability analysis

In the first part of the study, the compressibility and the stability of the monolayer has been analysed. This is done by calculating area per lipid (APL), phospholipids order parameter and density of the LSM components at different surface tensions. The APL value was calculated by measuring the average area of monolayer leaflet and dividing the number of lipid molecules.

3.1.1 Effect of surface tension on monolayer stability

To answer the question of how surface tension regulates monolayer compressibility and stability, the APL, lipids order parameter values and density profiles at different surface tensions were calculated in the absence and presence of a representative concentration (5.52%) of hydrocortisone, where the drug containing LSM is stable. Figure 2 reports changes of LSM

compressibility as a function of surface tension for drug-free and drug-containing monolayer. For the drug-free LSM, a consistent, surface tension-dependent increase in APL is observed from 0.486 ± 0.004 nm^2 at 0 mNm^{-1} surface tension to 0.613 ± 0.004 nm^2 at 50 mNm^{-1} surface tension.

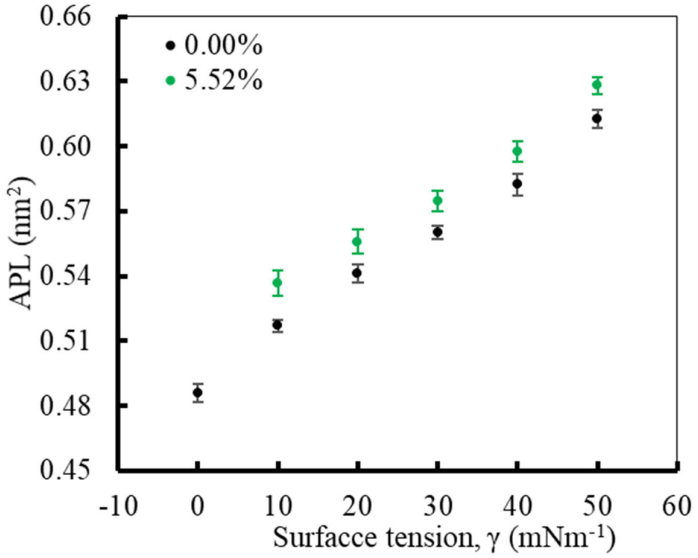

Figure 2. The APL values of the lung surfactant monolayer as a function of surface tension in the absence and presence of 5.52% w/w of glucocorticoid drug hydrocortisone for the surfactant protein containing monolayer. The error bars indicate standard deviation of the time evolution of APL data across the frames of the trajectories.

These APL values for drug-free monolayer is in agreement with the experimental value of APL found in previous studies of the comparable systems (surfactant protein-free monolayer) from atomistic and CG MD study investigated by Laing *et al*., [73], which are 0.527 ± 0.012 nm^2 and 0.545 ± 0.007 nm^2, respectively. In the presence of hydrocortisone, the APL values show similar concentration-dependent increase of APL from 0.537 ± 0.006 nm^2 at 10 mNm^{-1} surface tension to 0.628 ± 0.004 nm^2 at 50 mNm^{-1} surface tension with 99% confidence interval. It is notated that in the hydrocortisone containing system at 0 mNm^{-1} surface tension, the APL is not presented since at this surface tension, the drug causes the monolayer instability. The LSM starts engulfing the monolayer components by forming bilayer reservoir underneath the monolayer that induces the monolayer instability. In this state, the LSM shows small folding eventually causing monolayer collapse. The previously reported study shows such monolayer to bilayer transformation in a study of an LSM composed of DPPC:POPC:POPG:CHOL:SP-$B_{1\text{-}25}$:SP-C exposed to the corticosteroid drug mometasone [42].

As the surface tension induces LSM expansion, this is also likely affecting the conformational mobility of the lipid tails. Figure 3 illustrates the order parameter for the *sn*-1

and *sn*-2 chains of all phospholipids (DPPC, POPC and POPG) in the system calculated from simulations of surfactant protein containing monolayers, in the absence of corticosteroid drug hydrocortisone at surface tensions 0 to 50 mNm^{-1}. A consistent decrease of lipid order parameter with an increase of surface tension was observed for the saturated (DPPC, *sn*-1 and *sn*-2; POPC, *sn*-1 and POPG *sn*-1) and unsaturated (POPC, *sn*-2 and POPG *sn*-2) phospholipid chains. Thus, at 0 mNm^{-1} surface tension, the lipid tails are more ordered than at higher surface tension. This is consistent with the low APL values (Fig. 2) at low surface tension, reflecting highly packed lipids. This high order parameter shows that the monolayer is in liquid-condense (LC) phase [26]. The comparison of order parameter between saturated and unsaturated tails of the phospholipids reveals the expected lower order parameter for the unsaturated tails (*sn*-2 chain) of POPC and POPG compared to saturated tails (DPPC, *sn*-1 and *sn*-2; POPC, *sn*-1 and POPG *sn*-1) due to the presence of double bonds at D2-C3 bead (Fig. 3) in unsaturated chain. The surface tension dependent decrease of order parameters is also observed in the presence of 5.52% w/w hydrocortisone (supplementary Fig. S3). Overall, the order parameter analysis suggests that at surface tension 0 mNm^{-1}, the tails of the three phospholipids are highly orders and become less ordered with increasing surface tension.

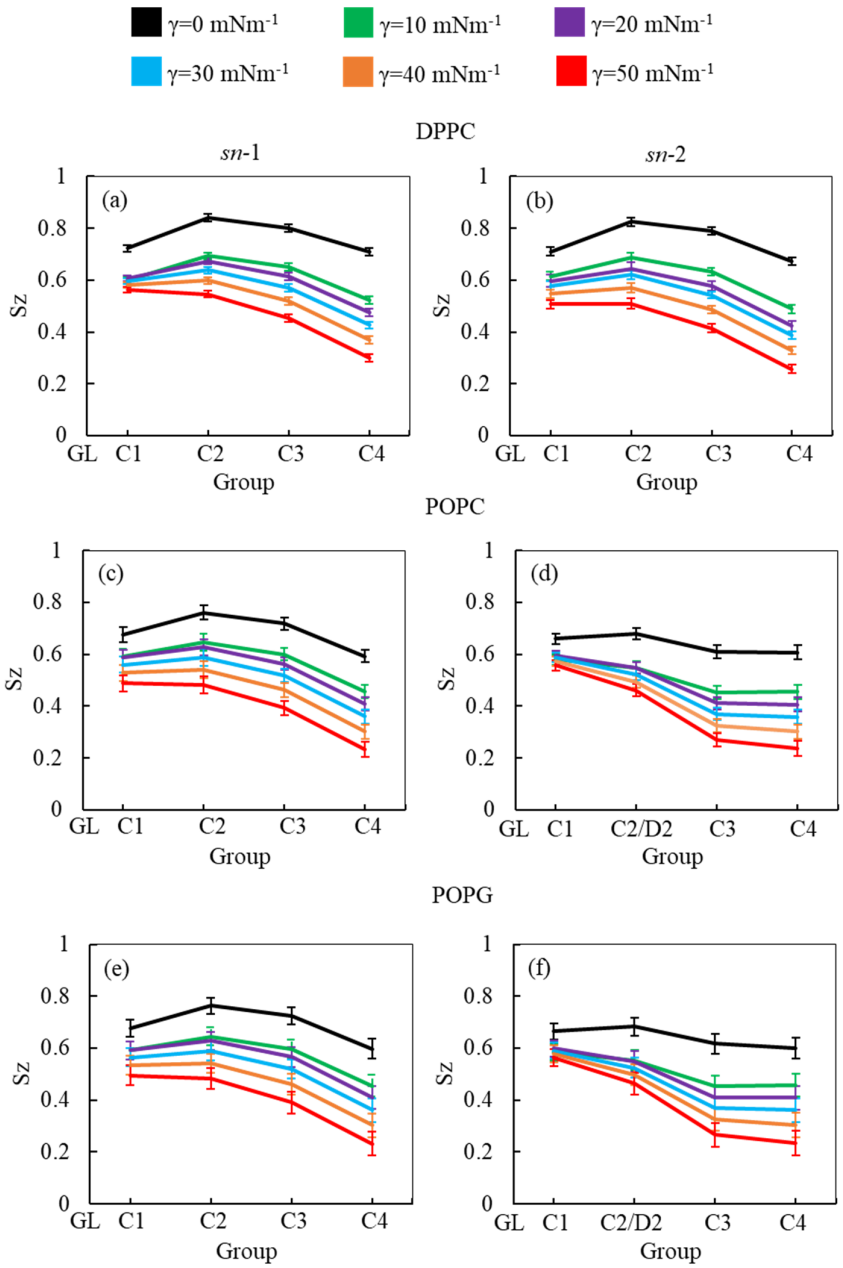

Figure 3. Order parameter of DPPC (a, b), POPC (c, d) and POPG (e, f) for *sn*-1 (a, c, e) and *sn*-2 (b, d, f) chains at different surface tension (0, 10, 20, 30, 40 and 50 mNm^{-1}) of drug-free protein containing monolayers. Order parameters were estimated for last one microsecond of the two microsecond simulations. The error bars denote standard deviations across the frames of the trajectories.

Mass density profiles of LSM components along the monolayer normal can be used to investiage whether the LSM is thinning or whether components are migrating away the lipid-water or lipid-air interface. Figure 4 shows the mass density profiles for the phospholipids and surfactant proteins from simulations at different surface tensions in the absence and presence

of 5.52% w/w hydrocortisone. For the drug-free monolayer, the comparison of density curves at the different surface tensions reveals that the peak heights of density curves at 0 mNm^{-1} surface tension are the furthest from the monolayer centre, while peak heights at 50 mNm^{-1} surface tension are the nearest. In addition, when surface tension increases, the peak height decreases. These differences suggest that at high surface tension, the monolayer is thinner than at low surface tension, which is consistent with the APL and order parameter data showing a more expanded monolayer at higher surface tension. In both systems (without and with) drug, the density curves are lifted along the monolayer centre, confirming the monolayer thinning.

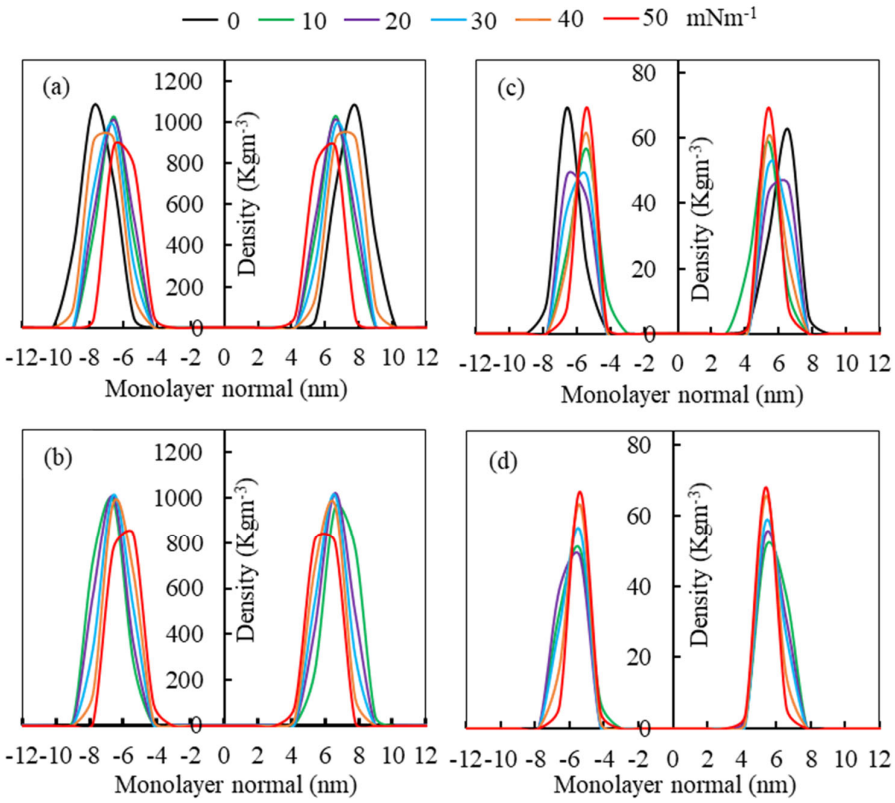

Figure 4. Mass density profiles of phospholipid (left pannels) and surfactant protein (right pannels) of the LSM. Comparison of density curves of LSM model at different surface tension in the absence (a, c) and presence (b, d) of 5.52% w/w hydrocortisone concentration.

The phospholipid density peak heights in the absence of drug (Fig. 4a) are 1.07, 1.02, 1.01, 0.98, 0.91 and 0.88 g cm^{-3}, and in the presence of drug (Fig. 4b), the attained peak heights are 0.98, 1.01, 1.02 g, 0.97 and 0.84 g cm^{-3} at surface tensions of 0, 10, 20, 30, 40 and 50 mNm^{-1}, respectively. These variations of density curves are noticeable for drug-free monolayer, whereas drug-containing monolayer shows less effect. The effect of surface tension on the

surfactant protein density profiles is also considerable in the drug containing monolayer, whereas there is no clear trend of protein density profiles for drug-free monolayer. These fluctuations of density are dependent of surface tension showing that there is a noticeable impact of surface tension on the lipid and protein density in the presence of drug. Overall, the findings of the density curves implies that the protein and drug exacerbate the surface tension-induced monolayer thinning. This is in line with the study by Islam *et al*., [42] for the corticosteroid drug mometasone.

3.1.2 Effect of hydrocortisone concentration on the pressure-area isotherm

The lateral expansion to the surfactant monolayer from a highly compressed (0.47 nm^2) monolayer to a highly expanded (0.61 nm^2) monolayer were applied to assess the effect of surface pressure and stability of the LSM in the absence and presence of hydrocortisone. The pressure-area (π-APL) isotherm curves in Fig. 5 shows that for all drug-free and drug-containing monolayers, the surface pressure decreases with increasing APL i.e., surface pressure is lower for a more expanded monolayer. While the overall trend is the same for drug-free and drug-containing monolayers, the absolute surface pressure is lower in the presence of the drug. A similar decrease in π-APL isotherm curves was found for the corticosteroid drugs budesonide and beclomethasone dipropionate [32].

Moving from the most expanded state (high APL) to the more condensed state (low APL), the monolayer passes through a monolayer-to-multilayer transition. As illustrated in the snapshots from the simulations, at lower APL, multilayered lipid folding starts occurring. If the monolayer is further compressed (<0.47 nm^2), then it is destabilised, and transform to lipid bilayer via the monolayer collapse. In the absence of drug, at an APL range of 0.47-0.51 nm^2, the monolayer exists in the LC phase according the Baoukina *et al.*, [56]. For molecular area 0.51 < APL ≤ 0.61 nm^2, the monolayer lies in the intermediate phase consisting of the combination of LC+LE phase. In this phase, the monolayer show different morphologies, structural and physicochemical features [26]. As the isotherms in Fig. 5 are decreasing with the increase of drug concentration at a certain range, the molecular-level data from simulations can be used to gain insight into lipid film organisation. In the presence of hydrocortisone, an intercalating action might occur in which hydrocortisone intercalates

between the phospholipid head groups, causing the monolayer components to pack more tightly. The decrease in APL shows that the phospholipid is becoming more compact, i.e., condense the monolayer at increasing drug concentration. In contrast to low APL, at APL > 0.61 nm^2, the monolayer is so expanded that starts pore formation. These pores are more pronounced in the presence of drug (Fig. S4). Wang *et al.*, [32] reported similar concentration-dependent effects of corticosteroids on the exogenous lung surfactant (Infasurf).

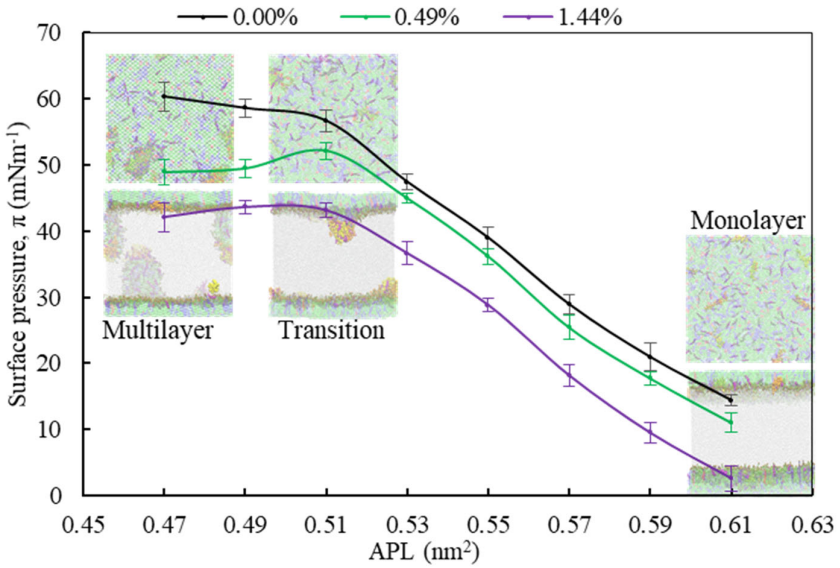

Figure 5. The effect of monolayer compression on the organisation of the lateral structure of LSM for increasing hydrocortisone concentartions by pressure-area (π-APL) isotherms calculation of the protein containing LSM of increasing hydrocortisone concentartions.

3.2 Structural and dynamical properties of monolayer at conditions mimicking exhalation and inhalation breathing

In the second part of the study, the systems were simulated at fixed surface tension of 0 and 20 mNm^{-1} at six different hydrocortisone contents from 0 to 10.46% w/w. These two surface tensions were considered to represent the extreme ends of exhalation (0 mNm^{-1}) and inhalation (20 mNm^{-1}) breathing conditions [9, 74].

3.2.1 Structural properties

We evaluated the APL values of the phospholipid monolayer for various hydrocortisone concentrations to investigate the influence of hydrocortisone on the compressibility of the monolayer. Fig. 6 shows the APL of the LSM for drug-free monolayers at four different hydrocortisone

concentrations for surface tension 20 mNm^{-1}. The calculated APL values are 0.541 ± 0.003, 0.543 ± 0.002. 0.548 ± 0.001, 0.556 ± 0.001 and 0.574 ± 0.002 nm^2 at drug concentrations of 0, 0.49, 1.44, 2.84 and 5.52% w/w, respectively.

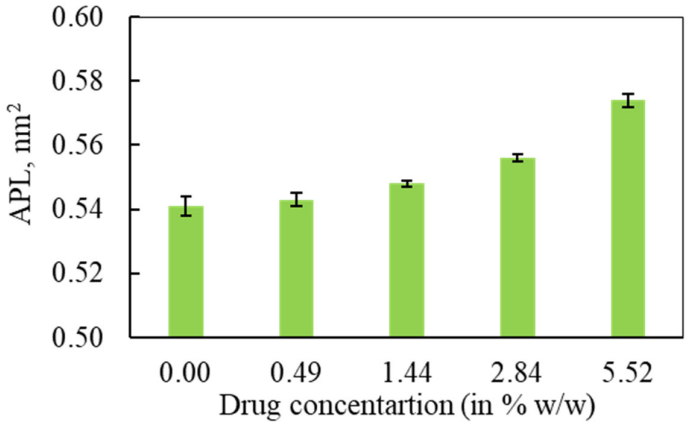

Figure 6. The effect of hydrocortisone concentration on the area per lipid (APL) from the simulation of protein containing system at 20 mNm^{-1}. The data were estimated over the last 1 µs of the 2 µs simulation. The error bar refers to standard deviations of the APL data across the frames.

The APL value for the drug-free monolayer agrees with the experimental value of APL (~0.50-0.70 nm^2) found in the literature as well as comparable system from atomistic [75] and CG simulation studies [73] at 20 mNm^{-1} surface tension by ~0.52 nm^2 and 0.55 nm^2, respectively. Hydrocortisone causes a considerable increase in compressibility of the monolayer. Such an increase in APL was previously reported for the corticosteroid drugs beclomethasone, budesonide and fluticasone [30]. When the drug concentration exceeds > 5.52% w/w then the additional drug molecules destabilise the monolayer and finally the monolayer collapses (Fig. S5). Such instability of the LSM is related to the increased fluidity in highly expanded monolayer, which was also reported by Zhang *et al*., [43] study.

In contrast to the compressibility (~0.54 nm^2) at 20 mNm^{-1} surface tension, the APL of LSM at 0 mNm^{-1} in the absence of drug and the presence of 0.49% w/w are estimated at 0.486 ± 0.004 nm^2 and 0.480 ± 0.004 nm^2, respectively. At 0 mNm^{-1} surface tension, the APL is not calculated for drug concentrations > 0.49% because at this surface tension the drug causes LSM instability and monolayer collapse (Fig. 7).

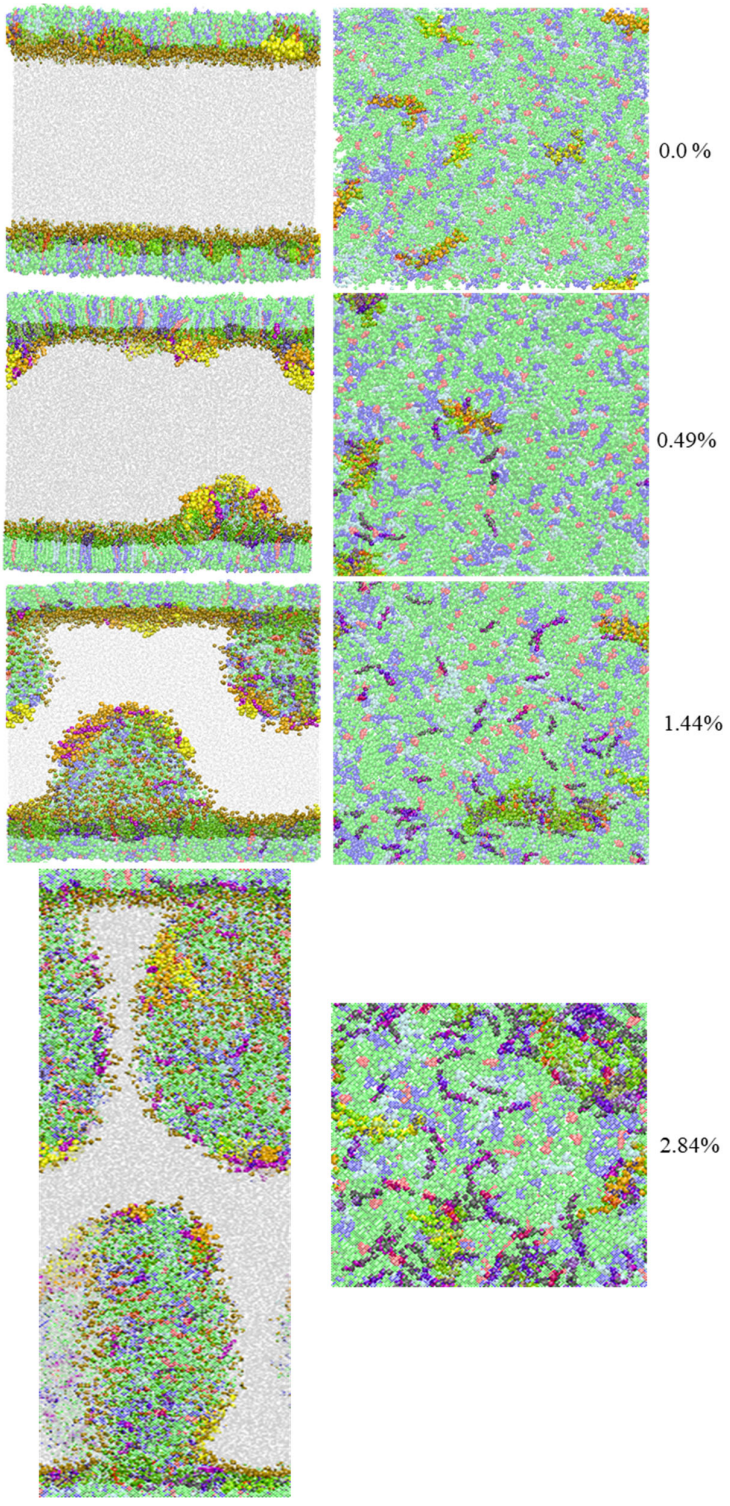

Figure 7. Snapshots of simulation system at surface tension 0 mNm^{-1} are shown in the absence and presence of increasing hydrocortisone concentrations of 0.49, 1.44, 2.84% w/w. Components are shown as DPPC (green), POPC (blue), POPG (cyan), CHOL (red), SP-B_{1-25}(orange), SP-C (yellow), cortisone (purple), water (silver), and phospholipids head groups (ochre).

To examine the minimum surface tension where the drug molecules do not destabilise (i.e., monolayer collapse) the LSM at given drug concentration, we repeated the simulation at surface tension from 1 to 5 mNm^{-1} at drug concentrations 0.49 to 5.52% w/w. The findings from these simulations implies that when surface tension ≥ 5 mNm^{-1}, there is no LSM collapse has been observed at higher drug concentration, which is consistent with the study conducted by Autilio *et al*., [12] for drug-free monolayer. To explore the collapsing mechanism at lower surface tension, the effect of surfactant protein was also investigated by simulation of the system in the absence and presence of surfactant protein. When APL values for drug-free and drug-containing monolayers are compared, it is obvious that surfactant protein has a major impact on monolayer compressibility. The effect of surfactant proteins can be found in the studies conducted by Islam *et al*., [42] and Duncan *et al*., [23]. The hydrophobic surfactant protein influences the lipid tails, potentially causing monolayer instability which is more pronounced in the presence of hydrophobic drug hydrocortisone. In both the absence and presence of hydrocortisone, it appears that the drug aids in the expansion of monolayers as compared to drug-free monolayers for all the underlying surface tensions. Such monolayer expansion can also be found in our recent publication for another corticosteroid drug mometasone [42].

In addition to APL calculation, phospholipid order parameter (*Sz*) informs about the structural changes of the monolayer by reporting the orientation of phospholipids chains in different phases (LC and LE). The phospholipids in LC phase are highly ordered producing higher order parameters, whereas in LE phase the phospholipids show lower order parameter values (see supplementary section S1.3 for detailed calculation). Figure 8 shows the phospholipids order parameters for DPPC, POPC and POPG from the simulation systems of DPPC-POPC-POPG-CHOL-SP-$B_{1\text{-}25}$-SP-C monolayer at surface tension 20 mNm^{-1} in the presence of increasing hydrocortisone concentrations. The order parameter for all three phospholipids (DPPC, POPC and POPG) decrease with increasing drug concentrations for both saturated and unsaturated phospholipid tails. Comparison between chain-1(*sn*-1) and chain-2 (*sn*-2) reveals that all unsaturated tails (POPC *sn*-2 and POPG *sn*-2) are less ordered than saturated chains (DPPC *sn*-1, DPPC *sn*-2, POPC *sn*-1 and POPG *sn*-1). This disordering of the phospholipids is because of the expansion of the monolayer surface area as shown in Fig. 6. Low drug concentrations of 0.49% and 1.44% w/w show a negligible effect on the order parameters.

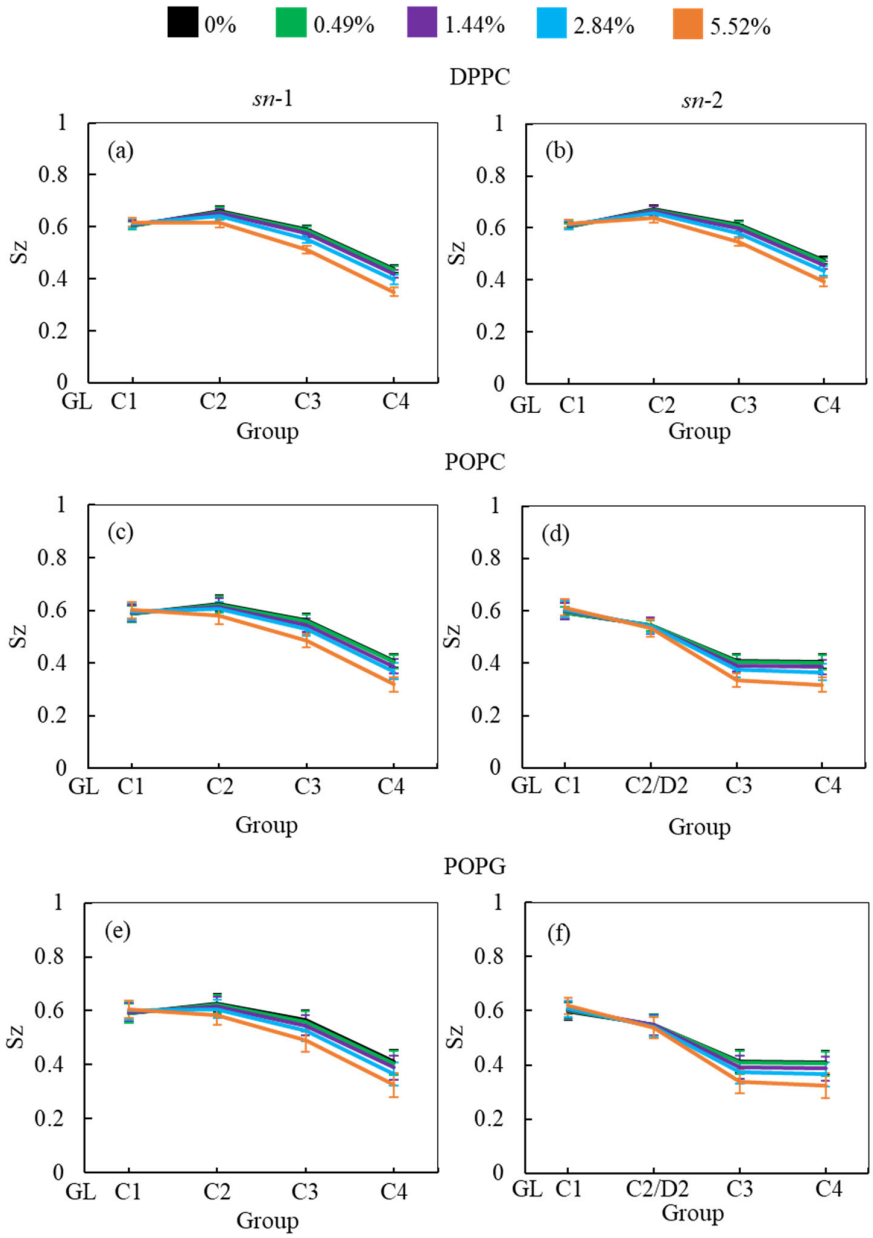

Figure 8. Concentration-dependent effect of hydrocortisone on the order parameter of (a, b) DPPC, (c, d) POPC, and POPG (e, f) for *sn*-1 (a, c, e) and *sn*-2 (b, d, f) chains at 20 mNm^{-1} surface tension. Order parameters were estimated for last one microsecond of the two microsecond simulations. The error bars were calculated across the frames of the simulation.

At 2.84% w/w of hydrocortisone, there is a decline in the order for DPPC, POPC and POPG at C2/D2-C3 and C3-C4 beads that gain drops for 5.52% w/w of hydrocortisone concentration. Simultaneously, the beads connecting GL-C1 and C1-C2/D2 show a small rise. The results in Fig. 8 indicate that drug molecules alter the phospholipids systematic arrangement in the LSM, which is substantially changes the physiological disordering at high drug concentrations (> 5.52%) and causes the LSM to collapse. In contrast to inhalation breathing (20 mNm^{-1} surface

tension), the incorporation of > 0.49% hydrocortisone at exhalation breathing condition (0 mNm^{-1} surface tension) the drug molecules significantly cause the lipids disordering and destabilise the monolayer. Overall, the APL and order parameters data revealed that hydrocortisone causes a concentration-dependent monolayer expansion causing the LSM disordering, with the effect being strongest at low surface tension.

3.2.2 Dynamical properties

3.2.2.1 Diffusion of the monolayer components and drug molecules

As listed in Table 2, the lateral diffusion coefficients of phospholipids (DPPC, POPC and POPG), cholesterol and surfactant proteins (SP-B and SP-C) in the mixed DPPC-POPC-POPG-CHOL-SP-B_{1-25}-SP-C monolayers for drug-free monolayers are $(6.11 \pm 0.61)\times10^{-7}$ cm^2 s^{-1}, $(5.47 \pm 0.01)\times10^{-7}$ cm^2 s^{-1}, $(2.36 \pm 0.71)\times10^{-7}$ cm^2 s^{-1} at surface tension 20 mNm^{-1}, respectively. The diffusion coefficients of phospholipids DPPC and POPC are $(7.0 \pm 2.0)\times10^{-7}$ cm^2s^{-1} and $(8.0 \pm 1.0)\times10^{-7}$ cm^2s^{-1}, respectively from existing *in silico* LSM modelling [48]. To the best of our knowledge, there are no experimental data regarding lateral diffusion coefficients of phospholipids for monolayers.

To assess the impact of corticosteroid drug hydrocortisone on the diffusion coefficient of phospholipids, cholesterol, protein and hydrocortisone itself, the diffusion coefficient at four different concentrations of hydrocortisone (0.49, 1.44, 284 and 5.52% w/w) were calculated , respectively as shown in Table 2. As it is observed from Table 2, when the drug concentration is increasing then the diffusion coefficient of phospholipids and cholesterol are decreasing from $(6.11 \pm 0.61)\times10^{-7}$ cm^2s^{-1} at drug-free LSM to $(4.32 \pm 0.30)\times10^{-7}$ cm^2s^{-1} at 5.52% w/w drug concentration and $(5.47 \pm 0.01)\times10^{-7}$ cm^2s^{-1} at drug-free LSM to $(3.51 \pm 0.94)\times10^{-7}$ cm^2s^{-1} at 5.52% w/w drug concentration for phospholipids and cholesterol, respectively. The diffusion coefficient of cholesterol at 20 mNm^{-1} surface tension for drug-free LSM shows agreement with Laing *et al.*, [73] study. In contrast to phospholipids and cholesterol diffusion coefficient, the diffusion coefficient of surfactant protein shows the opposite trend (increasing trend) with the increase of drug concentration. The estimated value of surfactant protein diffusion coefficient was $(2.36 \pm 0.71)\times10^{-7}$ cm^2s^{-1} at drug-free monolayer and $(5.42 \pm 0.41)\times10^{-7}$ cm^2s^{-1} at high drug concentration (5.52%). The incorporation of hydrocortisone molecules into the LSM hinders the spreading of the hydrocortisone itself that can be observed from the diffusion coefficient of hydrocortisone which are amounted to $(6.59 \pm 0.27)\times10^{-7}$ cm^2s^{-1}) at 0.49% and $(4.41 \pm 0.34)\times10^{-7}$ cm^2s^{-1} at 5.52% drug concentration. The diffusion coefficient of other

corticosteroid prednisolone was found $(6.0 \pm 4.0)\times10^{-7}$ cm^2s^{-1} that validates our calculated diffusion coefficient of hydrocortisone [48]. Overall, the dynamical properties of LSM components and corticosteroid drug by diffusion coefficient analysis demonstrates that the hydrophobic drug hinders the spreading rate of the phospholipids, cholesterol and the drug itself. On the other hand, the hydrocortisone influences the surfactant protein spreading.

Table 2. Diffusion coefficient (D, 10^{-7} cm^2s^{-1}) of the LSM components estimated from LSM model at 20 mNm^{-1}. Diffusion coefficients were estimated from the Einstein diffusion equation [76]. The diffusion coefficient was measured from entire 2 μs production run simulation. Errors represent standard deviations obtained from block averaging of the data from 20 fs time step.

Drug (in % w/w)	Phospholipids	Cholesterol	Protein	Hydrocortisone
0	6.11 ± 0.61	5.47 ± 0.01	2.36 ± 0.71	-
0.49	5.71 ± 0.12	5.30 ± 0.83	2.52 ± 0.52	6.59 ± 0.27
1.44	4.96 ± 0.34	4.96 ± 0.25	3.21 ± 0.45	5.03 ± 0. 16
2.84	4.67 ± 0.48	4.46 ± 0.56	4.73 ± 0.26	4.79 ± 0. 14
5.52	4.32 ± 0.30	3.51 ± 0.94	5.42 ± 0.41	4.41 ± 0. 34

3.2.2.2 Drug cluster formation

The adsorption of hydrocortisone drugs on the LSM can lead to cluster formation. To analyse the effect of hydrocortisone concentrations on the cluster formation of drug, the cluster size analysis of hydrocortisone was conducted for various hydrocortisone content at surface tension, γ = 20 mNm^{-1}. The number of hydrocortisone molecules in the system are 10 (for 0.49%), 30 (for 1.44%), 60 (for 2.84%) and 120 (for 5.52%) per monolayer. To compare the clustering between the different systems, the number of clusters were normalised to the number of drug molecules in the system at the lowest drug concentration. Figure 9 displays the normalised number of clusters and the number of hydrocortisone molecules in the largest cluster. For drug concentrations of 0.49, 1.44, 2.84, and 5.52% w/w, the time-averaged number of drug clusters were 9, 7, 6 and 3, respectively (Fig. 9a).

As seen in Fig. 9a, the number of clusters is decreasing with increasing drug concentration, which indicates the drug-drug interactions are less pronounced with higher drug concentration. The normalised number of drug molecules in the largest cluster are calculated 2, 1, 1 and 2 for drug concentrations 0.49, 1.44, 2.84 and 5.52%, respectively (Fig. 9b). The clusters are often stable throughout the simulation time up the hydrocortisone concentration 5.52% w/w over simulation time.

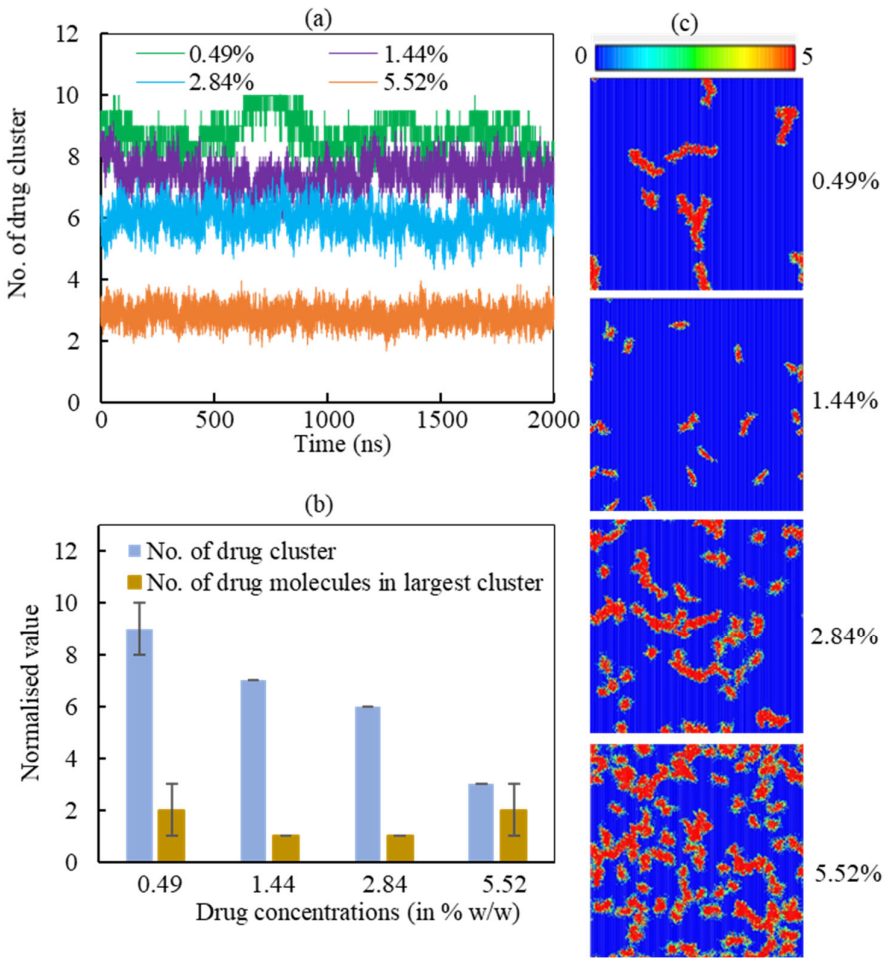

Figure 9. Normalised hydrocortisone cluster analysis four concentrations (0.49, 1.44, 2.84, 5.52% w/w) in the LSM at surface tension $\gamma = 20$ mNm^{-1}. (a) Number of hydrocortisone cluster formation over the time. (b) Number of normalised hydrocortisone cluster and the number of hydrocortisone molecules in the largest cluster are shown for different hydrocortisone concentrations. (c) The two-dimensional (2D) density map of the hydrocortisone to show the cluster formation on the monolayer at different hydrocortisone concentrations. The data was normalised using the number of drugs in the corresponding drug concentration with respect to the 0.49% w/w hydrocortisone concentration.

As it is seen from the simulation at drug concentration > 5.52% w/w, once the drug concentration exceeds 5.52%, then the excess hydrocortisone molecules help to destabilise the LSM and finally collapse the monolayer as shown in Fig. S5 in the supplementary material. Overall, the cluster analysis revealed that when drug concentration increases, there are fewer clusters, and these clusters are of roughly the same size for all simulated concentrations. The number of drugs in the largest cluster remains constant during the simulation time, indicating that on the timescale of the simulations, the drugs cannot disperse once they have aggregated. Nevertheless, as shown in the density maps, the number clusters present in the system clearly

increases with increasing concentrations. Thus, the destabilising effect seen for concentrations > 5.52% is not necessarily from an intrinsic change in clustering behaviour but the inability of breaking up these clusters in a short time frame. The lower number of cluster present at high drug concentrations that results the instability of the monolayer by faster drug spreading compared to monolayer expansion. This behaviour of drug clustering have also been reported for the steroid drug prednisolone by Estrada-López *et al*. [48] and mometasone by Islam *et al*. [42].

4. Implications

The interactions of corticosteroid drug hydrocortisone with LSM model appear to be very comparable to other corticosteroid drugs prednisone [48, 77, 78] or mometasone [42]. As a result of the structural similarities in corticosteroid drugs, it may be possible to generalise the fates of corticosteroids in lung surfactant. It is also worth noting that the interaction of corticosteroids with the lipids in the LSM is strong enough to keep them in the hydrophobic tail region of the phospholipids for the duration of the simulations (2 μs). Hydrocortisone can form nanoaggregates causing the LSM to collapse at the end of exhalation breathing condition. However, the proper spreading of the hydrocortisone molecules on the LSM can be observed in the inhalation breathing when the LSM is expanding. This spreading of hydrocortisone molecules is concentration-dependent and shows better spreading up to 5.52% w/w hydrocortisone. According to this investigation, hydrocortisone given in a certain critical concentration (10.46 % w/w) might cause the LSM damage. Lower concentrations of hydrocortisone, on the other hand, does not affect the LSM surface activity. The LSM has the characteristics of spreading hydrocortisone in a concentration-dependent manner and also dependent on the surface tension. The implications of this investigation will be used in pharmaceutical industry to develop an effective corticosteroids dose formulation for respiratory distress syndrome and the people with asthma or other lung diseases.

5. Limitations

In the simulation of various biomolecular processes, molecular modelling of biological systems using the molecular dynamics technique has shown significant progress [79]. However, molecular simulations have also limitations, just like any experiment or analytical procedure [80]. Considering the situation of lipid monolayers; there are issues with the computation of water surface tension and phospholipid monolayer surface pressure [81]. The phase separation of phospholipids monolayer from experiment that cannot be seen from simulation [82]. At low surface tension (< 2 mNm^{-1}), the phospholipid monolayers collapse, while at high surface

tension (more than 50 mNm^{-1}), a pore forms in the monolayer. The experimental data that is available is frequently limited or non-existent, difficult to obtain, and subject to significant fluctuations [83]. Nevertheless, there are situations when the discrepancy is attributable to a deficiency in the coarse-grained approach itself [84]. Our goal was to look at the partitioning and distribution of hydrocortisone in the LSM rather than the precise atomistic corticosteroid-lipid interactions. A CG model like MARTINI is appropriate for this application because it was designed with a specific focus on reproducing lipid partitioning behaviour [85]. Furthermore, our research included over 136 with 3 μs simulations, which are impossible to do with atomistic models. Steroids are frequently overly hydrophobic, which is one of the weaknesses of the model. Hydrocortisone partition coefficient is underestimated, implying that the free energy of partitioning is excessively negative. The relative partition coefficients for cortisone, mometasone, prednisolone, and cholesterol that we utilised as a reference are, however, accurate.

6. Conclusion

The stability of LSM interacting with corticosteroid drug hydrocortisone was effectively investigated using CG MD simulation. The structural details of the LSM were studied without and with hydrocortisone. In both the absence and presence of hydrocortisone, the drug appeared to assist in the enlargement of monolayers when compared to drug-free monolayers for applied interfacial tension of the LSM. The findings from constant-APL simulations show a continuous compression of the monolayer, and a concentration-dependent decrease in pressure-area isotherm curves, which replicates the surface pressure during normal breathing. An intercalating effect may occur, in which the hydrocortisone intercalates between the phospholipid head groups, causing the monolayer constituents to pack more closely at highly compressed monolayer. On the other hand, the findings from constant surface tension simulation mimicking inhalation and exhalation breathing condition imply that hydrocortisone produces a compression of the monolayer in a concentration-dependent manner that is more significant at exhalation breathing causing the LSM to collapse at >0.49 % w/w hydrocortisone concentration. For inhalation case, the drug-induced collapse was observed at higher hydrocortisone concentration (> 5.52%). The accumulation of drug molecule limits drug capacity to spread over the LSM at maximum drug contents, resulting in monolayer collapse. The results from the dynamical properties analysis demonstrate that larger clusters signal a lower drug capacity to

diffuse into the monolayer, which is significantly impeded when more drug molecules are present in the system. The findings from this investigation may help to better understand the interaction mechanism between inhaled corticosteroids and LSM, which will be helpful to pharmaceuticals to determine effective corticosteroid dosing for lung diseases.

Author contributions

M.Z.I. performed the simulations, formal data analysis, participated in the conceptualisation of the study and drafted the original manuscript. S.I.H. edited the manuscript. E.D. supervised M.Z.I. and critically revised the manuscript, and S.C.S. developed the concept, supervised M.Z.I. and edited the manuscript. All authors gave final approval for publication and agreed to be held accountable for the work performed therein.

Conflicts of interest

There are no conflicts to declare.

Acknowledgement

This work was conducted with the support of University of Technology Sydney (UTS) FEIT Research Scholarship and UTS International Research Scholarship (Mohammad Zohurul Islam). The computational facilities were provided by the UTS eResearch High-Performance Computer Cluster (HPCC) and National Computing Interface (NCI), Australia.

References

1. P. T. Daley-Yates, *British Journal of Clinical Pharmacology*, 2015, **80**, 372-380.
2. T. Rhen and J. A. Cidlowski, *New England Journal of Medicine*, 2005, **353**, 1711-1723.
3. P. J. Barnes, *Pharmaceuticals*, 2010, **3**, 514-540.
4. K. J. Rademaker, L. S. de Vries, C. S. Uiterwaal, F. Groenendaal, D. E. Grobbee and F. van Bel, *Archives of Disease in Childhood-Fetal and Neonatal Edition*, 2008, **93**, F58-F63.
5. I. P. Morris, N. Goel and M. Chakraborty, *European Journal of Pediatrics*, 2019, **178**, 1171-1184.
6. L. W. Doyle, R. A. Ehrenkranz and H. L. Halliday, *Neonatology*, 2010, **98**, 111-117.

7. M. W. Petersen, T. S. Meyhoff, M. Helleberg, M. B. N. Kjær, A. Granholm, C. J. S. Hjortsø, T. S. Jensen, M. H. Møller, P. B. Hjortrup and M. Wetterslev, *Acta Anaesthesiologica Scandinavica*, 2020, **64**, 1365-1375.

8. C. S. Kow and S. S. Hasan, *Cleve and Clinic Journal of Medicine*, 2020, **87**, 10.3949.

9. J. Perez-Gil and T. E. Weaver, *Physiology*, 2010, **25**, 132-141.

10. J. Goerke, *Biochimica et Biophysica Acta (BBA)-Molecular Basis of Disease*, 1998, **1408**, 79-89.

11. M. Chakraborty and S. Kotecha, *Breathe*, 2013, **9**, 476-488.

12. C. Autilio and J. Pérez-Gil, *Archives of Disease in Childhood-Fetal and Neonatal Edition*, 2019, **104**, F443-F451.

13. S. P. Caminiti and S. L. Young, *Hospital Practice*, 1990, **26**, 87-100.

14. E. J. Veldhuizen and H. P. Haagsman, *Biochimica et biophysica acta (bba)-biomembranes*, 2000, **1467**, 255-270.

15. E. Parra and J. Pérez-Gil, *Chemistry and Physics of Lipids*, 2015, **185**, 153-175.

16. R. Veldhuizen, K. Nag, S. Orgeig and F. Possmayer, *Biochimica et Biophysica Acta (BBA) - Molecular Basis of Disease*, 1998, **1408**, 90-108.

17. Y. Y. Zuo, R. A. Veldhuizen, A. W. Neumann, N. O. Petersen and F. Possmayer, *Biochimica et Biophysica Acta (BBA)-Biomembranes*, 2008, **1778**, 1947-1977.

18. A. G. Serrano and J. Pérez-Gil, *Chemistry and Physics of Lipids*, 2006, **141**, 105-118.

19. E. Lopez-Rodriguez and J. Pérez-Gil, *Biochimica et Biophysica Acta (BBA)-Biomembranes*, 2014, **1838**, 1568-1585.

20. R. Guagliardo, J. Pérez-Gil, S. De Smedt and K. Raemdonck, *Journal of Controlled Release*, 2018, **291**, 116-126.

21. S. Orgeig, P. S. Hiemstra, E. J. A. Veldhuizen, C. Casals, H. W. Clark, A. Haczku, L. Knudsen and F. Possmayer, *Respiratory Physiology & Neurobiology*, 2010, **173**, S43-S54.

22. J. Pérez-Gil, *Biochimica et Biophysica acta (BBA)-Biomembranes*, 2008, **1778**, 1676-1695.

23. S. L. Duncan and R. G. Larson, *Biochimica et Biophysica Acta (BBA)-Biomembranes*, 2010, **1798**, 1632-1650.

24. S. Schurch, H. Bachofen, J. Goerke and F. Possmayer, *Journal of Applied Physiology*, 1989, **67**, 2389-2396.

25. S. Baoukina, E. Mendez-Villuendas and D. P. Tieleman, *Journal of the American Chemical Society*, 2012, **134**, 17543-17553.

26. S. L. Duncan, I. S. Dalal and R. G. Larson, *Biochimica et Biophysica Acta (BBA)-Biomembranes*, 2011, **1808**, 2450-2465.

27. K. M. K. William Taeusch, H, *Pediatric Pathology & Molecular Medicine*, 2001, **20**, 519-536.

28. A. Cimato, G. Facorro and M. M. Sarrasague, *Respiratory Physiology & Neurobiology*, 2022, **296**, 103825.

29. B. Baer, L. McCaig, C. Yamashita and R. Veldhuizen, *Lung*, 2020, **198**, 909-916.

30. A. Cimato, G. Facorro and M. M. Sarrasague, *Respiratory Physiology & Neurobiology*, 2018, **247**, 80-86.

31. K. W. Lu, J. Goerke, J. A. Clements and H. W. Taeusch, *Pediatric Research*, 2005, **57**, 237-241.

32. Y. E. Wang, H. Zhang, Q. Fan, C. R. Neal and Y. Y. Zuo, *Soft Matter*, 2012, **8**, 504-511.

33. A. Cimato, G. Facorro and M. Martínez Sarrasague, *Respiratory Physiology & Neurobiology*, 2022, **296**, 103825.

34. A. G. Dos Santos, J. C. Bayiha, G. Dufour, D. Cataldo, B. Evrard, L. C. Silva, M. Deleu and M.-P. Mingeot-Leclercq, *Biochimica et Biophysica Acta (BBA)-Biomembranes*, 2017, **1859**, 1930-1940.

35. W. Daear, P. Lai, M. Anikovskiy and E. J. Prenner, *The Journal of Physical Chemistry B*, 2015, **119**, 5356-5366.

36. M. Javanainen, A. Lamberg, L. Cwiklik, I. Vattulainen and O. S. Ollila, *Langmuir*, 2018, **34**, 2565-2572.

37. A. Stachowicz-Kuśnierz, T. Seidler, E. Rogalska, J. Korchowiec and B. Korchowiec, *Chemosphere*, 2020, **240**, 124850.

38. J. Hu, X. Li, M. Li, Y. Shang, Y. He and H. Liu, *Colloids and Surfaces B: Biointerfaces*, 2020, **190**, 110922.

39. A. Bykov, G. Loglio, R. Miller, O. Milyaeva, A. Michailov and B. Noskov, *Colloids and Surfaces A: Physicochemical and Engineering Aspects*, 2019, **573**, 14-21.

40. K. Y. C. Lee, *Annu. Rev. Phys. Chem.*, 2008, **59**, 771-791.

41. F. Ravera, R. Miller, Y. Y. Zuo, B. A. Noskov, A. G. Bykov, V. I. Kovalchuk, G. Loglio, A. Javadi and L. Liggieri, *Current Opinion in Colloid & Interface Science*, 2021, **55**, 101467.

42. M. Z. Islam, S. I. Hossain, E. Deplazes and S. C. Saha, *Journal of Molecular Graphics and Modelling*, 2022, **111**, 108084.

43. H. Zhang, Y. E. Wang, C. R. Neal and Y. Y. Zuo, *Pediatric Research*, 2012, **71**, 316-323.

44. S. Meng, W. Cui, S. Lin, G. Wang, Y. Hei, B. Deng, S. Ma, Z. Zhang, Y. Liu and Y. Xie, *Journal of Chinese Pharmaceutical Sciences*, 2018, **27**, 415-428.

45. J. Hu, H. Liu, P. Xu, Y. Shang and H. Liu, *Langmuir*, 2019, **35**, 13452-13460.

46. S. Ortiz-Collazos, E. D. Estrada-López, A. A. Pedreira, P. H. Picciani, O. N. Oliveira Jr and A. S. Pimentel, *Colloids and Surfaces B: Biointerfaces*, 2017, **158**, 689-696.

47. F. Souza, F. Fornasier, L. Souza, M. Peñafiel, J. Nascimento, A. Malfatti-Gasperini and A. Pimentel, *Colloids and Surfaces A: Physicochemical and Engineering Aspects*, 2020, **584**, 124024.

48. E. D. Estrada-López, E. Murce, M. P. Franca and A. S. Pimentel, *RSC Advances*, 2017, **7**, 5272-5281.

49. S. Edsbäcker and C. J. Johansson, *Basic & Clinical Pharmacology & Toxicology*, 2006, **98**, 523-536.

50. T. A. Wassenaar, H. I. Ingólfsson, R. A. Böckmann, D. P. Tieleman and S. J. Marrink, *Journal of Chemical Theory and Computation*, 2015, **11**, 2144-2155.

51. S. I. Hossain, M. Z. Islam, S. C. Saha and E. Deplazes, *Methods in molecular biology (Clifton, N.J.)*, 2022, **2402**, 103-121.

52. S. J. Marrink, A. H. De Vries and A. E. Mark, *The Journal of Physical Chemistry B*, 2004, **108**, 750-760.

53. S. J. Marrink, H. J. Risselada, S. Yefimov, D. P. Tieleman and A. H. De Vries, *The Journal of Physical Chemistry B*, 2007, **111**, 7812-7824.

54. S. J. Marrink, A. H. de Vries, T. A. Harroun, J. Katsaras and S. R. Wassall, *Journal of the American Chemical Society*, 2008, **130**, 10-11.

55. S. O. Yesylevskyy, L. V. Schäfer, D. Sengupta and S. J. Marrink, *PLoS computational biology*, 2010, **6**, e1000810.

56. S. Baoukina, L. Monticelli, S. J. Marrink and D. P. Tieleman, *Langmuir*, 2007, **23**, 12617-12623.

57. L. Gordon, K. Lee, M. Lipp, J. Zasadzinski, F. Walther, M. Sherman and A. Waring, *The Journal of Peptide Research*, 2000, **55**, 330-347.

58. J. Johansson, T. Szyperski, T. Curstedt and K. Wuethrich, *Biochemistry*, 1994, **33**, 6015-6023.

59. J. Johansson and T. Curstedt, *Journal of Internal Medicine*, 2019, **285**, 165-186.

60. M. Sarker, A. J. Waring, F. J. Walther, K. M. Keough and V. Booth, *Biochemistry*, 2007, **46**, 11047-11056.

61. N. Biswas, S. Shanmukh, A. J. Waring, F. Walther, Z. Wang, Y. Chang, R. H. Notter and R. A. Dluhy, *Biophysical Chemistry*, 2005, **113**, 223-232.

62. V. Schram and S. B. Hall, *Biophysical Journal*, 2001, **81**, 1536-1546.

63. F. Baumgart, O. L. Ospina, I. Mingarro, I. Rodríguez-Crespo and J. Pérez-Gil, *Biophysical Journal*, 2010, **99**, 3234-3243.

64. J. Ding, D. Y. Takamoto, A. Von Nahmen, M. M. Lipp, K. Y. C. Lee, A. J. Waring and J. A. Zasadzinski, *Biophysical Journal*, 2001, **80**, 2262-2272.

65. M. Melo, H. Ingólfsson and S. Marrink, *The Journal of Chemical Physics*, 2015, **143**, 243252.

66. M. J. Abraham, T. Murtola, R. Schulz, S. Páll, J. C. Smith, B. Hess and E. Lindahl, *SoftwareX*, 2015, **1**, 19-25.

67. M. A. Cuendet and W. F. van Gunsteren, *The Journal of Chemical Physics*, 2007, **127**, 184102.

68. G. Bussi, D. Donadio and M. Parrinello, *The Journal of Chemical Physics*, 2007, **126**, 014101.

69. H. J. Berendsen, J. v. Postma, W. F. van Gunsteren, A. DiNola and J. Haak, *The Journal of Chemical Physics*, 1984, **81**, 3684-3690.

70. W. Humphrey, A. Dalke and K. Schulten, *Journal of Molecular Graphics*, 1996, **14**, 33-38.

71. S. J. Marrink, Martini Coarse Grain Forcefield for Biomolecules, http://cgmartini.nl/images/tools/do-order-gmx5.py, (accessed November 2020, 2020).

72. E. Boger and M. Fridén, *Journal of Aerosol Medicine and Pulmonary Drug Delivery*, 2019, **32**, 1-12.

73. C. Laing, S. Baoukina and D. P. Tieleman, *Physical Chemistry Chemical Physics*, 2009, **11**, 1916-1922.

74. S. Schürch, H. Bachofen and F. Possmayer, *Comparative Biochemistry and Physiology Part A: Molecular & Integrative Physiology*, 2001, **129**, 195-207.

75. S. L. Duncan and R. G. Larson, *Biophysical journal*, 2008, **94**, 2965-2986.

76. A. Einstein, *Annalen Der Physik*, 1905, **17**, 549-560.

77. M. Z. Islam, S. I. Hossain, E. Deplazes, S. Bhowmick and S. C. Saha, *AIP Conference Proceedings*, 2021, **2324**, 060008.

78. M. Z. Islam, M. Krajewska, S. I. Hossain, K. Prochaska, A. Anwar, E. Deplazes and S. C. Saha, *Langmuir*, 2022, DOI: 10.1021/acs.langmuir.1c02817.

79. W. Wang and R. Gómez-Bombarelli, *npj Computational Materials*, 2019, **5**, 125.

80. F. R. Souza, L. M. P. Souza and A. S. Pimentel, *Journal of Chemical Information and Modeling*, 2020, **60**, 5881-5884.

81. D. H. De Jong, S. Baoukina, H. I. Ingólfsson and S. J. Marrink, *Computer Physics Communications*, 2016, **199**, 1-7.

82. S. Baoukina and D. P. Tieleman, in *Biomolecular simulations*, Springer, 2013, vol. 924, pp. 431-444.

83. W. F. van Gunsteren, J. Dolenc and A. E. Mark, *Current Opinion In Structural Biology*, 2008, **18**, 149-153.

84. R. Alessandri, P. C. Souza, S. Thallmair, M. N. Melo, A. H. De Vries and S. J. Marrink, *Journal of Chemical Theory and Computation*, 2019, **15**, 5448-5460.

85. S. J. Marrink and D. P. Tieleman, *Chemical Society Reviews*, 2013, **42**, 6801-6822.